Sensors and Actuators A 303 (2020) 111655

Contents lists available at ScienceDirect

Sensors and Actuators A: Physical

journal homepage: www.elsevier.com/locate/sna

Thin-film bidirectional transducers for haptic wearables

Ian Trase [a], Zhe Xu [a], Zi Chen [a,**], Hong Tan [b], John X.J. Zhang [a,*]

[a] Thayer School of Engineering, Dartmouth College, 14 Engineering Drive, Hanover, NH, 03755, USA
[b] School of Electrical and Computer Engineering at Purdue University, West Lafayette, IN, 47907, USA

ARTICLE INFO

Article history:
Received 22 May 2019
Received in revised form 2 October 2019
Accepted 3 October 2019
Available online 9 October 2019

Keywords:
Haptics
Transducer
Thin-film
Wearables
Electrostatic
Flexible electrodes

ABSTRACT

We have designed, fabricated, and characterized a flexible electrostatic transducer (FET) for potential use as a wearable haptic actuator. This transducer both generates motion through the vibration of a curved electrode and measures the displacement of the same curved electrode to act as a displacement sensor. The transducer was analyzed through theory, simulation, and experiment to determine its displacement and sensing performance. It was found that a transducer with a footprint of 25 mm × 12.5 mm was able to generate displacements between 0.1 mm and 3.2 mm of displacement when operated at voltages between 25 V and 150 V. It was also capable of audible actuation at frequencies anywhere between 0.01 Hz and 10 kHz, including at target frequencies relevant to haptic communication. The transducer was able to sense changes to its shape through a change of capacitance, with a signal change of around 10% during maximum displacement. This sensing allows for both bidirectional communication and automatic displacement control through self-sensing. Simulation and theoretical results provide insight into the mechanism of actuation for the actuation and sensing systems, including predictions of displacement for a given voltage. User studies were also conducted, where it was found that the transducer generated perceivable and comfortable vibrations at both 26 Hz and 260 Hz, with 260 Hz being perceivable at lower amplitudes. The present work describes and characterizes a promising transducer for haptic communication.

1. Introduction

Haptic communication involves the bidirectional transmission of information through skin [1–3]. While current forms of remote communication are primarily auditory or visual, touch plays an underutilized role in face-to-face communication [4]. Touch is often used to communicate closeness or affection that are impossible through speech or writing. Human skin can also support the transmission of simple alphabets [5–8]. Vibration-based tactile feedback is common in smartphones as a typing aid [9–11], but its use is otherwise limited. A greater range of feedback is possible if the haptic communication system is directly mounted to skin [12,13] and exploits multiple touch modalities, such as vibration, stretch, and pressure [14–16]. Current devices suffer from large size [17–19], low force, or limited modalities [20]. Thin and flexible actuators provide an opportunity to shrink the device and generate multiple modalities, increasing information transfer [21–24].

Flexibility allows haptic actuators to conform to the skin as it stretches, shears, and twists. Flexible actuators are common in soft robotics, including actuators built from memory materials [25], pneumatic channels [26], dielectric elastomers [27], ionic polymer metal composites (IPMC) [28], and others [29]. Dielectric elastomers operate through electrostatics and are fast, flexible, and thin [30]. This has made them promising candidates for actuators in tactile feedback displays [31–33]. However, high voltages and low strain rates limit their application. Many micro-electromechanical (MEM) devices use electrodes that are not mechanically connected to generate larger strains at lower voltages [34]. Electrostatic MEM designs are promising for haptic communication, but the device must be scaled up and adapted for a flexible environment. At the microscale, large forces can be generated at low voltages, but only certain designs are scale-agnostic.

In this paper, we design thin and flexible electrostatic actuator-sensors using curved electrodes. The displacement of curved actuators with two clamped ends are measured for a range of voltages, geometries, and material properties. Theoretical predictions based on competition between bending and electrostatic energy are used to verify the experimental results, and COMSOL Multiphysics simulations are used to further confirm expected phenomena. Actuators are configured to deliver vibrotactile force to

* Corresponding author.
** Corresponding author.
E-mail address: john.zhang@dartmouth.edu (J.X.J. Zhang).

https://doi.org/10.1016/j.sna.2019.111655
0924-4247/

better exploit skin mechanoreceptors. The transducer also acts as a variable capacitor, with capacitance increasing with transducer compression.

The flexibility and low profile of our new actuator make it exceptionally well suited to haptics. We first describe the theory behind the transducers and provide predictions for actuation and sensing. We then detail construction of the transducers and characterize their actuation and sensing capabilities through both experiment and simulation. Finally, we conduct a user study to measure the percipibility and comfort of the transducers as haptic wearables.

2. Theory

2.1. Transducer description

A schematic of transducer operation is shown in Fig. 1a and b. The transducer consists of a pair of rectangular free-standing polymer thin films sputter-coated on one side with gold electrodes. The first film is fixed to a glass slide such that its gold electrode is in contact with the slide. The second film is attached to the first film such that the shorter sides of both films are in contact at either end and the gold electrode of the second film is oriented towards the first film. The second film is longer than the first, and it buckles into a cosine curve [35] with a height determined by the difference in length of the two films.

2.2. Actuation

When a voltage is applied across the electrodes, an attractive electrostatic force is generated between the buckled and rigid films. The force per unit length is proportional to the inverse of the separation between the films squared. Separation between films is high everywhere except for the points at which they are connected, where measurable force initially exists. As the electrostatic force pulls the buckled electrode into contact with the rigid film at these connection points, the separation between the two electrodes decreases. This creates a positive feedback loop where the decrease in film separation increases the electrostatic attraction, which further decreases the film separation. This phenomenon is equivalent to the "pull-in" effect experienced by many microelectromechanical systems [36]. In this transducer design, the runaway pull-in is countered by a mechanical restoring force that increases as the curved electrodes are deformed [37,38]. As the buckled film is pulled further from its stress-free shape, bending stress in the film increases until it is equal and opposite to the attractive electrostatic force. The transducer has either one or two stable equilibrium shapes for a given voltage, which can be predicted by balancing the bending force F_B and the electrostatic force F_E, described in Eq. 1 below. The electrostatic force can be simplified by assuming that the force is zero everywhere except the regions in which the two films are in contact.

$$F_E = \frac{w}{4\pi\varepsilon}\int_0^{L_R}\int_0^{L_B}\frac{\lambda_R(x)\lambda_B(s)y_B(s)}{\left([x-x_B(s)]^2+y_B^2(s)\right)^{\frac{3}{2}}}dsdx \rightarrow F_E \approx \frac{\varepsilon w L_C V^2}{2h^2},\ F_B = w\int_0^{L_B}\left[\sigma(s)*\hat{y}\right]ds\# \quad (1)$$

Here w is the width of the transducer, ε is the permittivity of the rigid polymer film, L_R is the total length of the rigid film, L_B is the total length of the buckled film, λ_R and λ_B are the charge distributions across the rigid and buckled films respectively, $y_B(s)$ and $x_B(s)$ are the x and y-coordinates of the buckled film with respect to the buckled film arc length s, L_C is the length of the buckled film that is in contact with the rigid film, V is the voltage across the two electrodes, h is the thickness of the rigid film, and $\sigma(s)$ is the Cauchy stress tensor of the buckled film. The actuation of the transducer is shown in a schematic in Fig. 1a.

The flexibility of the actuators allows them to easily deform in concert with the skin, and the mechanism of action works at any orientation or compression level. Because the mechanism of action is electrostatic, the response to an input signal is almost instantaneous and a simple AC voltage can drive the actuator. As both a positive and negative voltage will generate an attractive force, the driving frequency will be double that of an input AC signal. The transducer actuates visibly or audibly at input frequencies up to at least 10 kHz, which includes the 0 Hz–300 Hz range most relevant to human skin perception.

It is important to note the effects of scaling on the transducer. Assume the $L \times L$ footprint of the device shrinks while keeping film thickness and overall device height constant. The output force is proportional to L for a given displacement, and a smaller radius of curvature for the buckled beam would require a higher voltage for a given displacement. If, however, we reduce the thickness of the rigid insulating film as well, we can eliminate the requirement for a higher voltage. Thus, we can theoretically design transducers which can actuate at a given displacement for a variety of device footprints. The limiting factor when reducing the size of the transducer is the output force, which relates directly to perceptibility. Output force can be increased in a smaller transducer by increasing the rigidity of the buckled film (either by making it thicker or choosing a stiffer material), but at a certain point the force will become too small to feel. For this design of transducer, we estimate that it will remain perceptible when reduced in size to 5 mm × 5 mm.

2.3. Sensing

The rigid film and buckled film act as a variable parallel plate capacitor, where the capacitance changes based on the amount the transducer is compressed. During actuation the transducer only experiences force on the parts of the films that are in contact; likewise, the capacitance of the transducer is almost exclusively from the parts of the films that are in contact. By measuring this capacitance in real time, both the external pressure on the transducer and the shape of the transducer can be derived. This lets the transducer act as a haptic sensor, which is able to quantitatively sense human touch. In addition, it can be used in an automatic feedback loop to ensure actuating displacement height remains constant regardless of external forces on the transducer. The capacitance of the device is effectively that of a parallel plate capacitor, where the length of the parallel plate is equivalent to the length of the buckled film that is in contact with the rigid film. We can estimate the capacitance simply, as:

$$C_{max} = \frac{\varepsilon w L_C}{h}$$

Using $\varepsilon = 3.5\varepsilon_0$, $w = 10$mm, $L_C = 15$mm to 35mm, and $h = 25\mu$m, we can estimate that the measured capacitance of the devices ranges from around 186 pF to 434 pF.

The operation of the sensor is shown in Fig. 1b. One of the benefits of this kind of capacitive sensing is that it can detect both steady-state and transient pressure signals. Unlike unpowered sensing solutions, such as piezoelectric or triboelectric materials, the signal from a capacitive sensor does not degrade or change over time. The capacitance can be measured as a drop of voltage across the transducer when attached in series with a resistor and a capacitor of known value. A high frequency (e.g., 10–100 kHz, above skin's perception range) signal is sent through the circuit, and the measured voltage across the transducer will change based on its

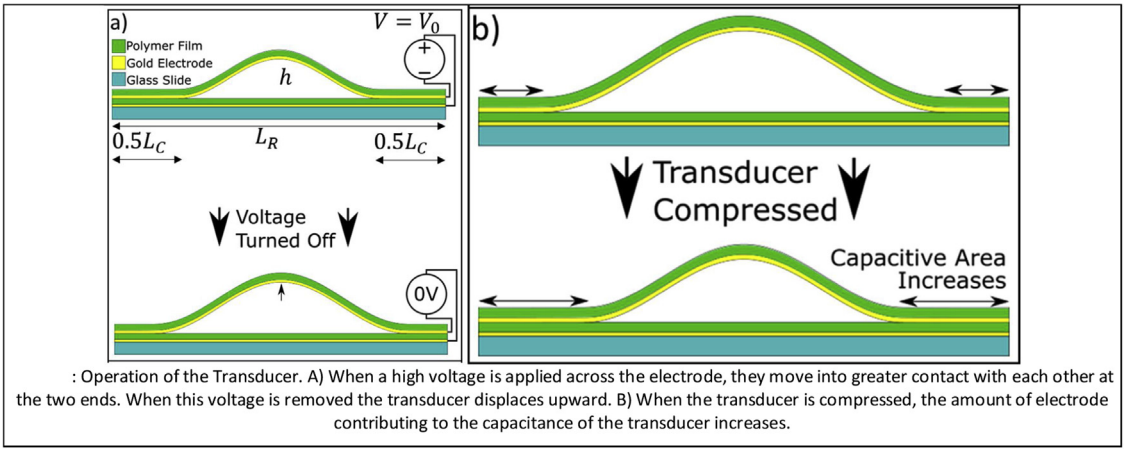

Fig. 1. Operation of the Transducer. A) When a high voltage is applied across the electrode, they move into greater contact with each other at the two ends. When this voltage is removed the transducer displaces upward. B) When the transducer is compressed, the amount of electrode contributing to the capacitance of the transducer increases.

capacitance. The ideal known capacitor for this kind of circuit is one close to the midpoint of the transducer capacitance range.

3. Experiment and simulation

3.1. Device fabrication

The actuators are composed of a flat film of thickness t_f fixed to a glass slide and a buckled 25 μm -thick Kapton film attached to either end of the flat film (Fig. 2a and b). The electrostatic force is highly dependent on t_f, so three different flat films were tested: a Kapton film with $t_f = 25\mu$m and two Mylar films with $t_f = 12\mu$m and $t_f = 2.5\mu$m. Both the flat and buckled films were sputtered with a 20 nm thick gold coating on the side closest to the glass slide. Mylar and Kapton were chosen as they both have excellent dielectric strength and are good insulators, thus reducing the chance of device breakdown. Each film had a small extra rectangle of gold electrode, to which a wire was attached with a small piece of conductive copper tape. These wires were connected in turn to either a high voltage amplifier for the actuation experiments or to a signal generator for the sensing experiments. The buckled flat film was fixed to the rigid film with a piece of scotch tape on one end and was lightly fixed by a piece of removable silicone. This fabrication process is summarized in Fig. 2c. This silicone could be removed and adjusted to change the length of the buckled film and thus the height of the device. Lastly, a small piece of white tape was adhered to the highest point of the buckled film, to improve the ability of the laser vibrometer to measure the film motion.

3.2. Actuation experiments

The transducers can be induced to actuate when driven by a high-voltage signal. Each transducer was hooked up to the output of a Trek model 2210 high voltage amplifier with a gain of 100, the input of which was connected to a Keysight 33522B signal generator. The transducer was vertically mounted to a 3-axis stage fixed to an optical table, as shown in Fig. 3. As the transducer actuates electrostatically, it will ideally move in the same manner for positive and negative voltages. To prevent any changes in actuation that could be the result of stray electrical charge buildup on either film, a custom positive-only signal was created (Fig. 3). This signal ramped up from 0 to 5 V over the course of 5 s at a specified frequency. Three input frequencies of 10 Hz, 20 Hz, and 40 Hz were tested. A Polytech PDV-100 laser vibrometer was mounted to the optical table and aimed at the small piece of white tape on the transducer. This vibrometer was connected to a desktop computer through the Polytech Vibtech software to determine the real-time displacement. When the signal generated was used with the custom input signal, the transducer actuated and the changes in displacement of the buckled film were recorded by the laser vibrometer.

Devices of several different heights and rigid film thicknesses were tested. Films of 25μm Kapton, 12.5μm Mylar, and 2.5μm Mylar were tested, and heights of 1 mm to 6 mm were tested. In addition, a 12.5μm transducer was tested at a wide range of frequencies to determine the frequency response and a rough estimate of the damping coefficient. The vibrometer displacement output was processed using MATLAB to extract a plot of maximum center-point displacement vs voltage at each of the three chosen frequencies, the three film thicknesses, and the two gap heights. A Butterworth lowpass filter was used to reduced signal noise, and displacements at each voltage were extracted using peak detection. All devices tested were 25 mm by 10 mm in size.

3.3. Sensing experiments

To determine how the change in capacitance was related to the change in shape, a simple circuit and testing setup was constructed. The circuit consisted of a 10kΩ resistor and a 235pF capacitor in series with the device and a signal generator, shown in the photograph in Fig. 4. The capacitor was chosen to have a capacitance approximately the same as the capacitance of the transducer when half-compressed, as this would allow for the largest dynamic range in terms of voltage change. An AC signal with an amplitude of 10 V and frequency of 1 kHz was sent through the circuit, and the voltage across the device was measured. As the device was compressed, the capacitance rose, shown through a drop of voltage. We can correlate this voltage drop with a change in device shape, allowing us to sense deformation. An additional benefit of this sensing method is that it can theoretically be used in tandem with actuation, allowing for device self-sensing. A sliding stage was used to slowly compress the device, and the resulting signal was recorded through an oscilloscope, shown in Fig. 4. The stage was moved in 1 mm increments, up to a max of 16 mm. Each transducer had 7.5 mm of the buckled film permanently in contact with the rigid film on each side, which gave the device an initial capacitance even when completely uncompressed. Devices of three different film types (25μm Kapton, 12.5μm Mylar, and 2.5μm Mylar) and 4 different heights were tested, for a total of 12 devices.

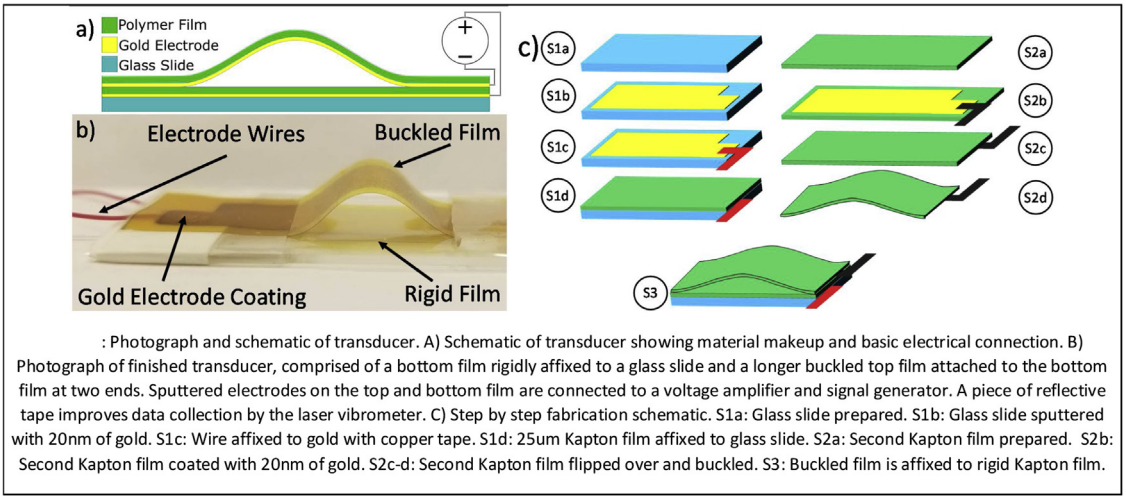

: Photograph and schematic of transducer. A) Schematic of transducer showing material makeup and basic electrical connection. B) Photograph of finished transducer, comprised of a bottom film rigidly affixed to a glass slide and a longer buckled top film attached to the bottom film at two ends. Sputtered electrodes on the top and bottom film are connected to a voltage amplifier and signal generator. A piece of reflective tape improves data collection by the laser vibrometer. C) Step by step fabrication schematic. S1a: Glass slide prepared. S1b: Glass slide sputtered with 20nm of gold. S1c: Wire affixed to gold with copper tape. S1d: 25um Kapton film affixed to glass slide. S2a: Second Kapton film prepared. S2b: Second Kapton film coated with 20nm of gold. S2c-d: Second Kapton film flipped over and buckled. S3: Buckled film is affixed to rigid Kapton film.

Fig. 2. Photograph and schematic of transducer. A) Schematic of transducer showing material makeup and basic electrical connection. B) Photograph of finished transducer, comprised of a bottom film rigidly affixed to a glass slide and a longer buckled top film attached to the bottom film at two ends. Sputtered electrodes on the top and bottom film are connected to a voltage amplifier and signal generator. A piece of reflective tape improves data collection by the laser vibrometer. C) Step by step fabrication schematic. S1a: Glass slide prepared. S1b: Glass slide sputtered with 20 nm of gold. S1c: Wire affixed to gold with copper tape. S1d: 25um Kapton film affixed to glass slide. S2a: Second Kapton film prepared. S2b: Second Kapton film coated with 20 nm of gold. S2c-d: Second Kapton film flipped over and buckled. S3: Buckled film is affixed to rigid Kapton film.

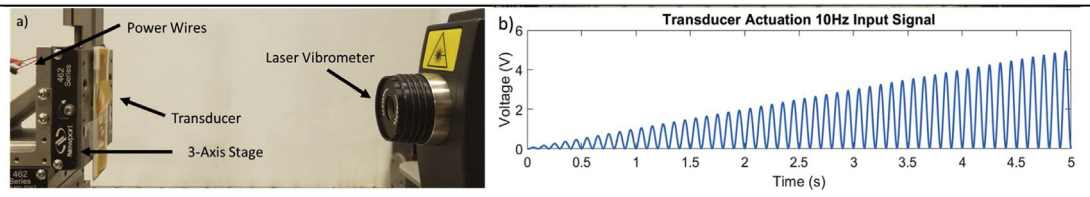

: Schematic of laser vibrometer setup and actuator driving signal. A) The laser vibrometer (right) is aimed at the actuator (left), which is fixed to a 3-axis stage. The actuator is connected to a voltage amplifier and signal generator, while the laser vibrometer feeds velocity data to a lab computer. B) A sample signal from the signal generator. The signal is 5 seconds long, positive for its duration, and is 10 (shown), 20, or 40Hz. The voltage rises and falls linearly to account for any hysteresis in the device.

Fig. 3. Schematic of laser vibrometer setup and actuator driving signal. A) The laser vibrometer (right) is aimed at the actuator (left), which is fixed to a 3-axis stage. The actuator is connected to a voltage amplifier and signal generator, while the laser vibrometer feeds velocity data to a lab computer. B) A sample signal from the signal generator. The signal is 5 s long, positive for its duration, and is 10 (shown), 20, or 40 Hz. The voltage rises and falls linearly to account for any hysteresis in the device.

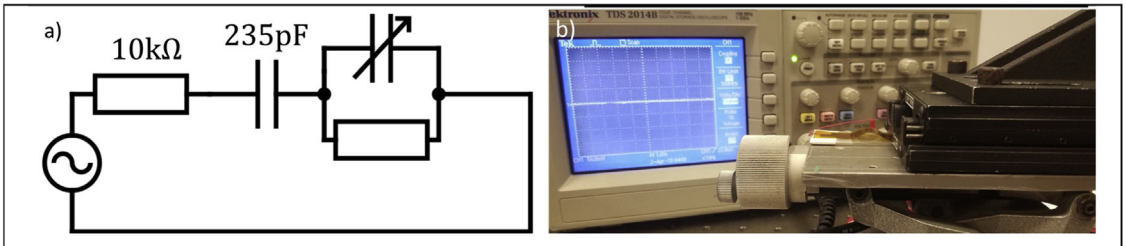

: Transducer sensing system. A) Schematic of sensor circuit for capacitance measurement, with transducer modeled as a resistor and capacitor in parallel. B) Photograph of sensing setup with horizontal stage for transducer compression and oscilloscope for voltage measurement.

Fig. 4. Transducer sensing system. A) Schematic of sensor circuit for capacitance measurement, with transducer modeled as a resistor and capacitor in parallel. B) Photograph of sensing setup with horizontal stage for transducer compression and oscilloscope for voltage measurement.

3.4. Simulations

Electromechanical nonlinear 2D simulations of the airgap device were performed using COMSOL to predict and verify the measured displacement. The film was modeled with tetragonal elements for precision while the air under the film was modeled with a rough mapped mesh to increase simulation speed (Fig. 5). To ensure that shear of the mapped mesh elements remained small throughout deformation, element anchor points were algorithmically determined and manually prescribed. To couple the solid mechanic deformation and the static charge distribution, a moving mesh calculated using Yeoh smoothing was assigned to the air under the buckled film. Devices of the same rigid film thicknesses were tested (25 μm, 12 μm, and 2.5 μm), and gap heights were tested from 1 mm to 6 mm in increments of 0.5 mm. Each study prescribed a center point displacement and calculated the shape of the film and voltage required to reach this displacement. The center point dis-

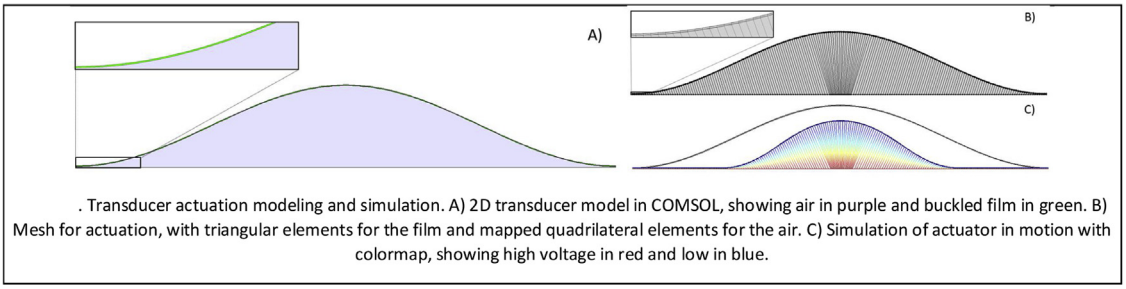

Fig. 5. Transducer actuation modeling and simulation. A) 2D transducer model in COMSOL, showing air in purple and buckled film in green. B) Mesh for actuation, with triangular elements for the film and mapped quadrilateral elements for the air. C) Simulation of actuator in motion with colormap, showing high voltage in red and low in blue. (For interpretation of the references to colour in this figure legend, the reader is referred to the web version of this article).

placements ranged from 0 mm to either the gap height or to the point where the buckled film would self-intersect.

3.5. User studies

To test the efficacy of the newly designed FET on the skin, we conducted an IRB-approved study to measure the comfort and perceptibility of the device at different voltages and frequencies. Ten participants between the ages of 21–27, 50% female, had the FET placed on the top (dorsal) or bottom (volar) side of their forearm with a piece of nitrile glove acting as an extra insulator. During the experiment, a voltage signal was sent out through a PC 3.5 mm audio jack, amplified through an op-amp circuit and the high-voltage amplifier and sent to the FET. MATLAB was used to send and record the audio signals and all subject responses. Along with the two arm locations, 2 frequencies (26 Hz and 260 Hz) were compared. During the tests, a vibration was generated randomly in one of 3 intervals. If the subject could feel the vibration 3 times in a row, the voltage was decreased by either 1.5 dB or 0.5 dB depending on the duration of the trial. If they got it wrong once, the voltage was increased by the same amount. This procedure, called three-interval, one-up three-down adaptive procedure in psychophysics [39], allowed us to zero-in on the threshold of detection. Lastly, we also measure the threshold at which the vibration became uncomfortably intense for each of the 4 conditions.

4. Results and discussion

4.1. Actuation experiments

Fig. 6 shows cross-sections of the resulting data, including voltage vs. displacement, gap height vs. displacement, bottom film thickness vs. voltage, and frequency vs. displacement. Devices with larger gap heights tend to have larger maximum displacements, as expected, but also have smaller displacements at lower voltages. All the devices have a characteristic “turn-on” voltage, below which they move very little. Once this turn-on voltage is reached, the displacement will rise rapidly with voltage and then level off. At low voltages, the electrostatic force is too small to pull in the closest part of the buckled film. After the turn-on voltage is reached a positive feedback loop occurs. When a piece of the buckled film contacts the base, it moves the rest of the buckled film closer, which increases the electrostatic force. The increased force pulls in more of the film, and this cycle continues until the reaction bending force of the buckled film becomes large enough to balance the electrostatic force. The bending force rises quickly at high voltages, which makes it difficult to fully compress the buckled film and accounts for the leveling off in the voltage-displacement curve.

A larger gap-height will result in a higher turn-on voltage, as a larger initial distance between the films requires greater electrostatic force to close the gap. Larger gap heights also lead to higher rates of displacements after the turn-on voltage. The force per mm of displacement is relatively similar between devices of different gap-heights, so taller devices experience rapid increases in displacement as they move from the turn-on voltage displacement to the “standard” displacement for that voltage. As the bottom film thickness decreases, the turn-on voltages become compressed. Thus, a device with a gap height of 2 mm would turn on at 200 V with a film thickness of 25 μms but only 50 V with a film thickness of 2.5 μms. The frequency of the driving signal has little effect on the displacement. The displacement dropped to low levels at frequencies well above our range of interest (»50 Hz), but displacements were similar between 10,20, and 40 Hz. At these low frequencies, the displacement is approximately equal to the displacement at a 0HZ DC signal. In other words, the device acts as a lowpass filter with a cutoff frequency above 100 Hz.

The devices were capable of both symmetric up-down and asymmetric side-to-side motion. The side-to-side motion resulted in larger detected center-point displacement and is a good candidate for haptic actuation, as the skin is more sensitive to shear force. In addition, the side-to-side motion may be less sensitive to the position of the device on the skin. Devices were constructed where only half of the top film was electroded, thus forcing the film to move side-to-side under applied voltage.

We additionally performed experiments to determine the frequency response of the transducer. It was found that the transducer had a small resonance when supplied by a driving signal of around 50 Hz, and displacement decreased significantly after 500 Hz (Fig. 7). This corresponds to a true resonance of around 100 Hz, as the transducer doubles the frequency of any AC driving signal with 0 DC component. Thus, a driving signal of 50 Hz causes the transducer to actuate at 100 Hz. The cutoff frequency, at which the displacement had dropped by 3 dB, was measured to be 1000 Hz (500 Hz driving signal). The device used for this experiment had a maximum height of 2 mm, a 25-micron insulator thickness, and was run at 400 V (200 V to −200 V). The maximum displacement of the device (before normalization) was 0.7 mm at a 50 Hz driving signal. The transducer actuation remained audible as a pure tone all the way up to 10,000 Hz, indicating that motion was significant even at high frequencies. As a haptic transducer, only the frequencies below 1000 Hz are relevant, and at these frequencies, displacement remains high.

We also performed an impulse test, where a 3 Hz square wave with a 10% duty cycle and 0 V–350 V range was used to drive the transducer. This allowed us to measure the damping of the motion and get a rough estimate of the damping coefficient. Using a resonant frequency of 100 Hz, we estimated a damping coefficient of around 0.7 kg/s and a damping ratio of around 0.9, near critical damping. The effective spring constant for the device is highly nonlinear, depending on the voltage, the displacement, and the distance and properties of the skin in contact. Thus, the damping coefficient as well is a function of voltage, displacement, and fre-

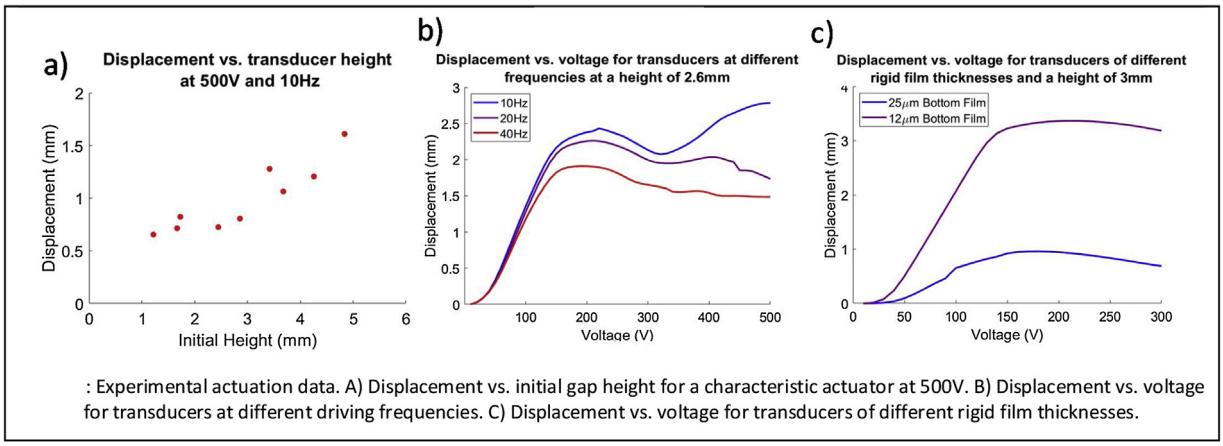

Fig. 6. Experimental actuation data. A) Displacement vs. initial gap height for a characteristic actuator at 500 V. B) Displacement vs. voltage for transducers at different driving frequencies. C) Displacement vs. voltage for transducers of different rigid film thicknesses.

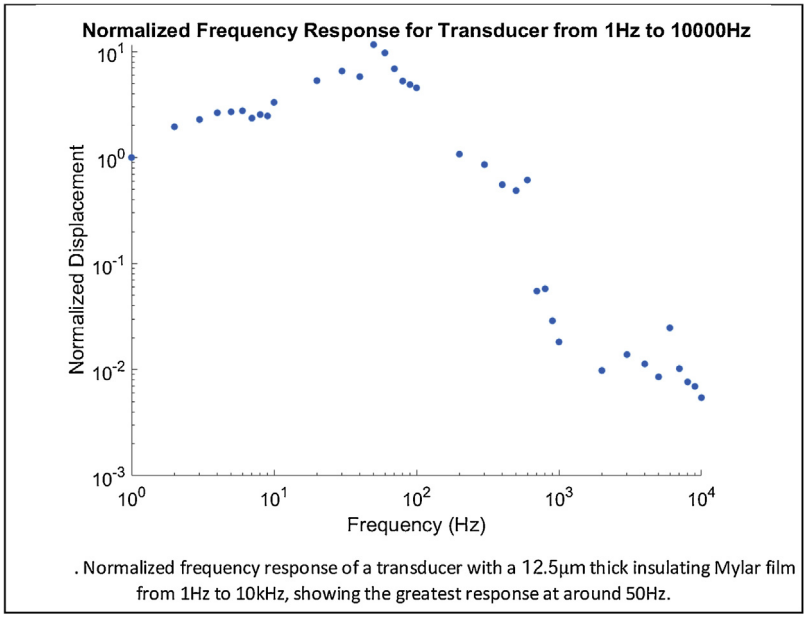

Fig. 7. Normalized frequency response of a transducer with a 12.5μm thick insulating Mylar film from 1 Hz to 10 kHz, showing the greatest response at around 50 Hz.

quency of the driving signal. The estimate of 0.7 kg/s applies to the device at low frequencies and standard voltages, and deviations from these parameters will change the damping as well.

4.2. Sensing experiments

The results of the sensing experiments are summarized in Fig. 8 . It was found that neither transducer height nor rigid film thickness has a significant effect on the percentage change of capacitance when the transducer is compressed. The capacitance of the transducer is based solely on the amount of the rigid film that is in contact with the buckled film. The height of the buckled film above the rigid film should have no effect on capacitance – a transducer with a height of 6 mm should have approximately the same capacitance of a transducer with a height of 1 mm. Similarly, the thickness of the rigid film will influence the absolute magnitude of the transducer's capacitance, but not on the percentage change. A film that is twice as thin will have a capacitance that is twice as large, but the maximum and minimum capacitance will still differ by around 10%. A thinner film is advantageous as it increases the sensitivity of the transducer by increasing the capacitance range. The resilience of these sensing measurements to changes in device shape indicate that the transducer will be able to reliably sense haptic deformation on the skin with little calibration necessary.

4.3. Simulations

The data obtained from the simulations is summarized in Fig. 9. In the low-voltage regime (0–500 V), the simulations corroborated the results of the experiments. A clear turn-on voltage was noted, the rate of displacement increase was higher for devices with larger airgaps, and as the bottom film thickness decreased, the turn-on voltages became compressed. The simulations were able to run to much higher voltages than the experiments, allowing us to view new trends. Because the simulations monotonically increase displacement rather than voltage, they correctly model situations in which the voltage decreases as displacement increases. Larger gap heights require a lower voltage than their turn-on voltage for a large part of their prescribed displacements. This indicates that the physical devices snap from the shape at the turn-on voltage to a

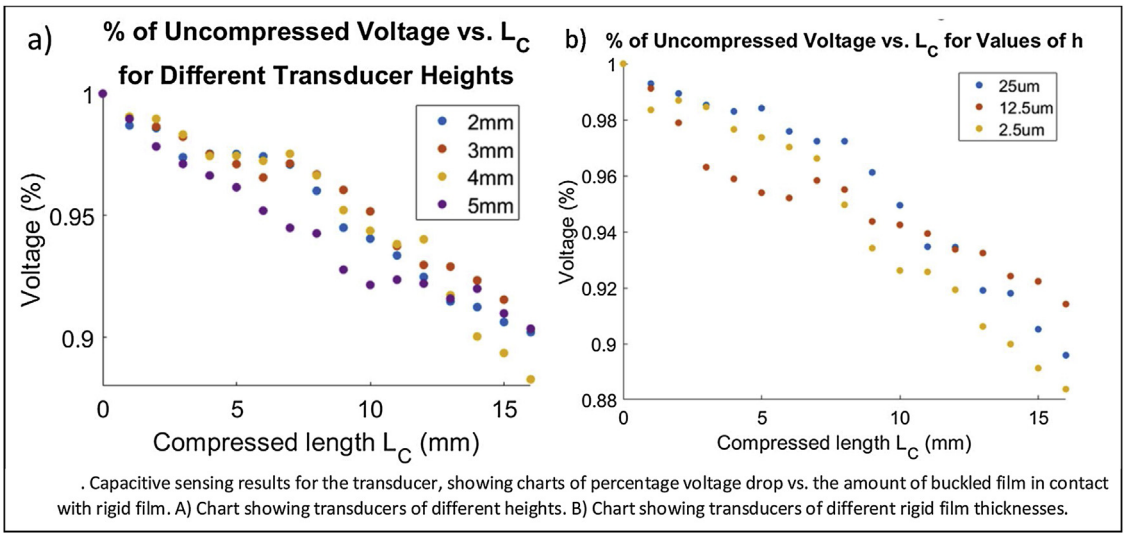

Fig. 8. Capacitive sensing results for the transducer, showing charts of percentage voltage drop vs. the amount of buckled film in contact with rigid film. A) Chart showing transducers of different heights. B) Chart showing transducers of different rigid film thicknesses.

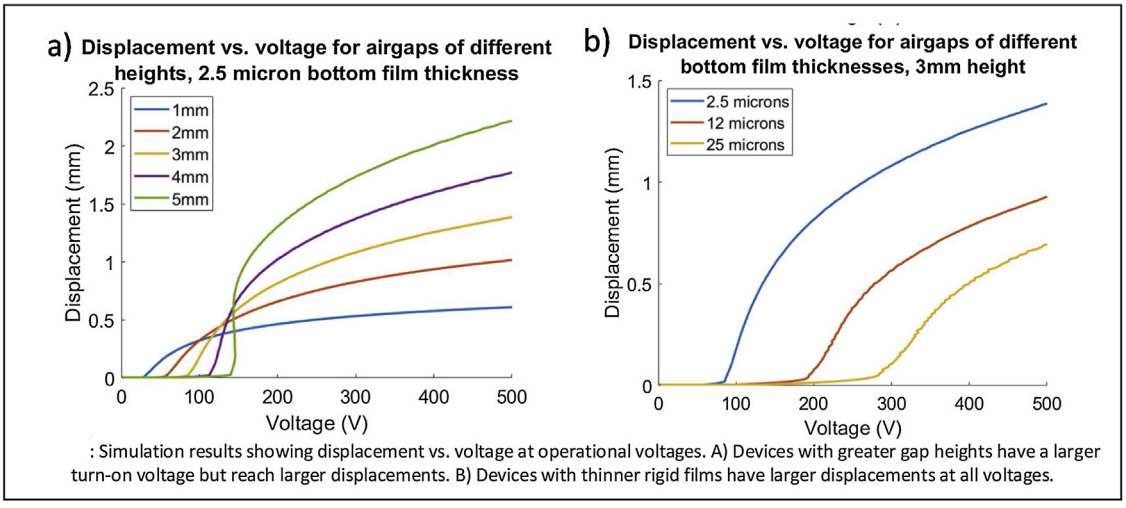

Fig. 9. Simulation results showing displacement vs. voltage at operational voltages. A) Devices with greater gap heights have a larger turn-on voltage but reach larger displacements. B) Devices with thinner rigid films have larger displacements at all voltages.

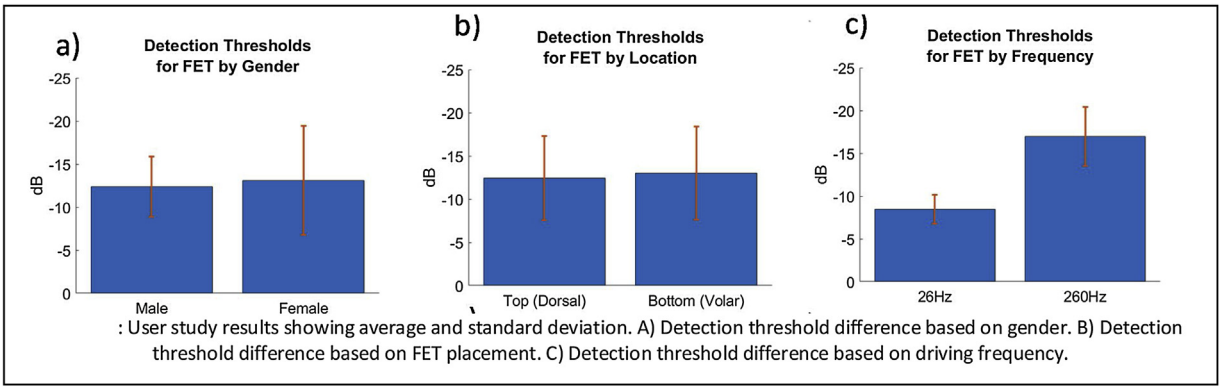

Fig. 10. User study results showing average and standard deviation. A) Detection threshold difference based on gender. B) Detection threshold difference based on FET placement. C) Detection threshold difference based on driving frequency.

much higher displacement. This phenomenon is known as bistability, as there are a set of voltages at which the device can exist and be stable at either of two displacements. The buckled films of devices with small air gaps become completely flat and compressed at high voltages, resulting in an ultimate decrease in required voltage. The buckled films of devices with larger airgaps instead become pinched (Fig. 9b).

While experiments and simulations were qualitatively similar and had displacements of the same order of magnitude, experiments registered higher displacements than the simulations. The most likely explanation for the discrepancy is the introduction of asymmetrical deformation modes. While the simulation was constrained to be symmetric, the buckled films of the experimental devices could move side-to-side. Side-to-side motion registers as a higher displacement, as the laser vibrometer only tracks center-point displacement.

4.4. User studies

The results from the user studies are summarized in Fig. 10. The data indicate that neither gender nor location has a strong effect on FET vibration perception, with average detection thresholds for all configurations averaging around -12.5 dB. Frequency has a very strong effect, as reported in the literature [40]. The detection threshold for the 26 Hz signal averaged around -8 dB, while the threshold for the 260 Hz signal was -17 dB. The decibel threshold values are combinations of the driving voltage and the frequency-dependent actuator displacement response, with 0 dB set to the displacement of a 1000 V signal driven at 26 Hz. The fact that perception is not affected by location or gender means that it will need less calibration and setup in the field. We believe that this result is a function of the sharp voltage turn-on effect seen in the laser vibrometer and simulation experiments. Because the FET increases in amplitude very quickly in a narrow voltage range, the thresholds of detection should fall within this narrow range. The human skin is naturally much more sensitive to high frequency vibrations vs. low frequency vibrations, which accounts for the difference in detection threshold at the two frequencies tested.

5. Conclusion

We developed a viable haptic electrostatic transducer capable of effectively delivering information to and receiving information from the skin. The transducer is lightweight, flexible, and durable. We conducted experimental prototyping to characterize and optimize the device, as well as simulations to better understand the mechanics. It was found that the transducer was able to reach displacements of over 3 mm when driven by a 10 Hz 150 V signal, with frequencies viable up to around 10 kHz. The transducer sensing signal changed by around 10% between full displacement and zero displacement, which indicates that the device will have a favorable dynamic range and sensitivity when applied for self-sensing. Finally, we conducted a user study to prove the efficacy of these devices in a real-world environment, in which it was found that the transducer was perceivable and comfortable at both 26 Hz and 260 Hz on multiple forearm locations. The experiments, simulations, and user studies showed that it was possible to build and operate these devices at voltages under 500 V, paving the way for improved systems for future haptic communications.

Declaration of Competing Interest

The authors have no competing interests to declare.

Acknowledgements

The authors are grateful for the financial support of the National Science Foundation award (ECCS1509369), the National Institute of Health (NIH) Director's Transformative Research Award (R01HL137157), the Thayer School of Engineering PhD Innovation Program, and Facebook, Inc. under the SARA program. Z.C. acknowledges the support from the Branco Weiss–Society in Science Fellowship, administered by ETH Zürich.

References

[1] A. Haans, W. IJsselsteijn, Mediated social touch: a review of current research and future directions, Virtual Real. 9 (2006) 149–159, http://dx.doi.org/10.1007/s10055-005-0014-2.
[2] C.M. Reed, H.Z. Tan, Z.D. Perez, E.C. Wilson, F.M. Severgnini, J. Jung, J.S. Martinez, Y. Jiao, A. Israr, F. Lau, K. Klumb, R. Turcott, F. Abnousi, A phonemic-based haptic display for speech communication, IEEE Trans. Haptics 12 (2019) 2–17.
[3] L.A. Jones, Tactile communication systems: optimizing the display of information, Prog. Brain Res. 192 (2011) 113–128, http://dx.doi.org/10.1016/B978-0-444-53355-5.00008-7.
[4] I. Morrison, L.S. Löken, H. Olausson, The skin as a social organ, Exp. Brain Res. 204 (2010) 305–314, http://dx.doi.org/10.1007/s00221-009-2007-y.
[5] M. Enriquez, K. MacLean, C. Chita, Haptic phonemes: basic building blocks of haptic communication, Proc. 8th Int. Conf. Multimodal Interfaces (2006) 302–309, http://dx.doi.org/10.1145/1180995.1181053.
[6] L.M. Brown, S.A. Brewster, H.C. Purchase, A first investigation into the effectiveness of tactons, Proc. - 1st Jt. Eurohaptics Conf. Symp. Haptic Interfaces Virtual Environ. Teleoperator Syst. World Haptics Conf. WHC 2005 (2005) 167–176, http://dx.doi.org/10.1109/WHC.2005.6.
[7] F.A. Geldard, Adventures in tactile literacy, Am. Psychol. 12 (1957) 115–124, http://dx.doi.org/10.1037/h0040416.
[8] G. Luzhnica, E. Veas, V. Pammer, Skin reading: encoding text in a 6-channel haptic display, Proc. 2016 ACM Int. Symp. Wearable Comput. (2016) 148–155, http://dx.doi.org/10.1145/2971763.2971769.
[9] E. Hoggan, S.A. Brewster, J. Johnston, Investigating the effectiveness of tactile feedback for mobile touchscreens, Proc. SIGCHI Conf. Hum. Factors Comput. Syst. (CHI' 08) (2008) 1573–1582, http://dx.doi.org/10.1145/1357054.1357300.
[10] M. Fukumoto, T. Sugimura, Active click: tactile feedback for touch panels, Proc. CHI 2001 (Extended Abstr. (2001) 121–122, http://dx.doi.org/10.1145/634067.634141.
[11] Zhaoyuan Ma, D. Edge, L. Findlater, H.Z. Tan, Haptic keyclick feedback improves typing speed and reduces typing errors on a flat keyboard, 2015 IEEE World Haptics Conf. (2015) 220–227, http://dx.doi.org/10.1109/WHC.2015.7177717.
[12] G. Huisman, A. Darriba Frederiks, B. Van Dijk, D. Hevlen, B. Krose, The TaSSt, Tactile sleeve for social touch, 2013 World Haptics Conf. WHC 2013 (2013) 211–216, http://dx.doi.org/10.1109/WHC.2013.6548410.
[13] A. Gallace, H.Z. Tan, C. Spence, The body surface as a communication system: the state of the art after 50 years, Presence Teleoperators Virtual Environ. 16 (2007) 655–676, http://dx.doi.org/10.1162/pres.16.6.655.
[14] Z. Fan Quek, S.B. Schorr, I. Nisky, W.R. Provancher, A.M. Okamura, Sensory substitution and augmentation using 3-degree-of-freedom skin deformation feedback, IEEE Trans. Haptics 8 (2015) 209–221, http://dx.doi.org/10.1109/TOH.2015.2398448.
[15] N. Dunkelberger, J. Sullivan, J. Bradley, N.P. Walling, I. Manickam, G. Dasarathy, A. Israr, F.W.Y. Lau, K. Klumb, B. Knott, F. Abnousi, R. Baraniuk, M.K. O'Malley, Conveying language through haptics: a multi-sensory approach, in: Proc. 2018 ACM Int. Symp. Wearable Comput, 2018, pp. 25–32.
[16] N. Colella, M. Bianchi, G. Grioli, A. Bicchi, M.G. Catalano, A novel skin-stretch haptic device for intuitive control of robotic prostheses and avatars, IEEE Robot. Autom. Lett. 4 (2019) 1572–1579, http://dx.doi.org/10.1109/LRA.2019.2896484.
[17] A.A. Stanley, K.J. Kuchenbecker, Design of body-grounded tactile actuators for playback of human physical contact, 2011 IEEE World Haptics Conf. (2011) 563–568, http://dx.doi.org/10.1109/WHC.2011.5945547.
[18] S. Choi, K.J. Kuchenbecker, Vibrotactile display: perception, technology, and applications, Proc. IEEE. 101 (2013) 2093–2104, http://dx.doi.org/10.1109/JPROC.2012.2221071.
[19] L.A. Jones, Perspectives on the evolution of tactile, haptic, and thermal displays, Presence Teleoperators Virtual Environ. 25 (2016) 247–252.
[20] Y.-W. Park, S.-H. Bae, T.-J. Nam, How do couples use CheekTouch over phone calls? Proc. 2012 ACM Annu. Conf. Hum. Factors Comput. Syst. - CHI' 12. (2012) 763, http://dx.doi.org/10.1145/2207676.2207786.
[21] A. Marette, A. Poulin, N. Besse, S. Rosset, D. Briand, H. Shea, Flexible zinc–tin oxide thin film transistors operating at 1 kV for integrated switching of dielectric elastomer actuators arrays, Adv. Mater. 29 (2017) 1–6, http://dx.doi.org/10.1002/adma.201700880.
[22] S. Rosset, H.R. Shea, Flexible and stretchable electrodes for dielectric elastomer actuators, Appl. Phys. A Mater. Sci. Process. 110 (2013) 281–307, http://dx.doi.org/10.1007/s00339-012-7402-8.
[23] M. Mohiuddin, H.U. Ko, H.C. Kim, J. Kim, S.Y. Kim, Transparent and flexible haptic actuator based on cellulose acetate stacked membranes, Int. J. Precis. Eng. Manuf. 16 (2015) 1479–1485, http://dx.doi.org/10.1007/s12541-015-0196-9.
[24] I.H. Trase, Z. Xu, Z. Chen, H.Z. Tan, J.X.J. Zhang, Flexible electrostatic transducers for wearable haptic communication, in: Proc. World Haptics Conf. 2019, 2019, p. submitted.

[25] A. Villoslada, A. Flores, D. Copaci, D. Blanco, L. Moreno, High-displacement flexible shape memory alloy actuator for soft wearable robots, Rob. Auton. Syst. 73 (2015) 91–101, http://dx.doi.org/10.1016/j.robot.2014.09.026.
[26] Ching-Ping Chou, B. Hannaford, Measurement and modeling of McKibben pneumatic artificial muscles, IEEE Trans. Robot. Autom. 12 (1996) 90–102, http://dx.doi.org/10.1109/70.481753.
[27] K. Jung, J.C. Koo, J. Do Nam, Y.K. Lee, H.R. Choi, Artificial annelid robot driven by soft actuators, Bioinspir. Biomim. 2 (2007), http://dx.doi.org/10.1088/1748-3182/2/2/S05.
[28] C. Zheng, S. Shatara, X. Tan, Modeling of robotic fish propelled by an ionic polymer-metal composite caudal fin, Proc. SPIE - Int. Soc. Opt. Eng. 7287 (2009) 689–694, http://dx.doi.org/10.1117/12.815789.
[29] M. Karpelson, R. Pena, R.J. Wood, Low-cost electromechanical actuator arrays for tactile display applications, 2018 IEEE Int. Conf. Robot. Autom (2018) 471–476, http://dx.doi.org/10.1109/ICRA.2018.8460909.
[30] C. Keplinger, J.-Y. Sun, C.C. Foo, P. Rothemund, G.M. Whitesides, Z. Suo, Stretchable, transparent, ionic conductors, Science 80 (341) (2013) 984–987, http://dx.doi.org/10.1126/science.1240228.
[31] M. Matysek, H. Haus, H. Moessinger, D. Brokken, P. Lotz, H.F. Schlaak, Combined Driving and Sensing Circuitry for Dielectric Elastomer Actuators in Mobile Applications, 797612, 2011, pp. 797612, http://dx.doi.org/10.1117/12.879438.
[32] M. Matysek, P. Lotz, T. Winterstein, H.F. Schlaak, Dielectric elastomer actuators for tactile displays, Proc. - 3rd Jt. EuroHaptics Conf. Symp. Haptic Interfaces Virtual Environ. Teleoperator Syst. World Haptics 2009 (2009) 290–295, http://dx.doi.org/10.1109/WHC.2009.4810822.
[33] M. Matysek, P. Lotz, K. Flittner, H.F. Schlaak, Vibrotactile Display for Mobile Applications Based on Dielectric Elastomer Stack Actuators, 2010, pp. 76420D, http://dx.doi.org/10.1117/12.847358.
[34] D.J. Bell, T.J. Lu, N.A. Fleck, S.M. Spearing, MEMS actuators and sensors: observations on their performance and selection for purpose, J. Micromech. Microeng. 15 (2005), http://dx.doi.org/10.1088/0960-1317/15/7/022.
[35] L.D. Landau, E.M. Lifshitz, Theory of Elasticity, 3rd ed., Pergamon Press, Oxford, 1986.
[36] W.M. Zhang, H. Yan, Z.K. Peng, G. Meng, Electrostatic pull-in instability in MEMS/NEMS: a review, Sens. Actuators A Phys. 214 (2014) 187–218, http://dx.doi.org/10.1016/j.sna.2014.04.025.
[37] R. Jebens, W. Trimmer, J. Walker, Microactuators for aligning optical fibers, Sens. Actuators 20 (1989) 65–73, http://dx.doi.org/10.1016/0250-6874(89)87103-3.
[38] R. Legtenberg, J. Gilbert, S.D. Senturia, M. Elwenspoek, Electrostatic curved electrode actuators, J. Microelectromech. Syst. 6 (1997) 257–265, http://dx.doi.org/10.1109/84.623115.
[39] L.A. Jones, H.Z. Tan, Application of psychophysical techniques to haptic research, IEEE Trans. Haptics 6 (2013) 268–284, http://dx.doi.org/10.1109/TOH.2012.74.
[40] S.J. Bolanowski, G.A. Gescheider, R.T. Verrillo, C.M. Checkosky, Four channels mediate the mechanical aspects of touch, J. Acoust. Soc. Am. 84 (1988) 1680–1694, http://dx.doi.org/10.1121/1.397184.

Biographies

Ian Trase received his Bachelor's degree in Mechanical Engineering from Princeton University in 2014 with certificates in Materials Science and Engineering Physics. Ian's research experiences include internships at the Princeton Electric Propulsion Laboratory and MIT CSAIL. He is currently a pH.D. Innovation Fellow at the Thayer School of Engineering at Dartmouth, where his research focuses on flexible electronics and wearable haptics with an interest in translating technologies out of the lab to commercial applications.

Zhe Xu received his M.S. (2014) degree and Ph.D. (2017) degree from Erik Jonsson School of Engineering and Computer Science at University of Texas at Dallas, Dallas, Texas. Currently he is a research associate of Professor John X.J. Zhang in Thayer school of Engineering at Dartmouth College, Hanover, New Hampshire. His research interest lies at piezoelectric composite materials, bio-inspired materials, advanced manufacture, Implantable energy harvesting application, and bio-integration of soft electronics.

Dr. Zi Chen is an Assistant Professor at Thayer School of Engineering at Dartmouth, an Adjunct Assistant Professor in the Department of Biological Sciences, and a PI at Dartmouth's Norris Cotton Cancer Center. He received his bachelor's and master's degree in Materials Science and Engineering from Shanghai Jiaotong University, and a PhD in Mechanical and Aerospace Engineering from Princeton University. Dr. Chen's research has been supported by NIH, Society in Science, and American Academy of Mechanics, and he has received the Society in Science-Branco Weiss Fellowship. He has published over 50 peer reviewed journal papers and filed two US patents.

Hong Z. Tan received her Bachelor's degree in Biomedical Engineering from Shanghai Jiao Tong University and earned her Master and Doctorate degrees, both in Electrical Engineering and Computer Science, from the Massachusetts Institute of Technology (MIT). She was a Research Scientist at the MIT Media Lab from before joining the faculty at Purdue University in 1998. She is currently a professor of Electrical and Computer Engineering, with courtesy appointments in the School of Mechanical Engineering and the Department of Psychological Sciences at Purdue University. Her research focuses on haptic human-machine interfaces, taking a perception-based approach to solving engineering problems.

John X.J. Zhang is a Professor at Thayer School of Engineering, Dartmouth College, and an Investigator of Dartmouth-Hitchcock Medical Center. He received his Ph.D. from Stanford University, and was a Research Scientist at Massachusetts Institute of Technology. Dr. Zhang is a Fellow of American Institute for Medical and Biological Engineering, and a recipient of NIH Director's Transformative Research Award, NSF CAREER Award, DARPA Young Faculty Award, Facebook SARA award, Sony Faculty Innovation Award and many other recognitions. Zhang's research focuses on exploring bio-inspired nanomaterials, scale-dependent biophysics, and nanofabrication technology, towards developing new diagnostic devices, implantable bioenergy harvesting systems and wearable soft transducers.